DOI: 10.16539/j.ddgzyckx.2018.01.010

卷(Volume)42, 期(Number)1, 总(SUM)162
页(Pages)150~162, 2018, 2(February, 2018)

大地构造与成矿学
Geotectonica et Metallogenia

羌塘雀莫错始新世石英二长岩的年代学、地球化学与岩石成因

曾纪鹏[1,2], 王　强[1*], 欧　权[1], 齐　玥[1], 郝露露[1],
孙　鹏[1], 王　军[1], 陈怡伟[1]

(1.中国科学院 广州地球化学研究所 同位素地球化学国家重点实验室, 广东 广州 510640; 2.中国科学院大学, 北京 100049)

摘　要: 正长岩以及富碱的石英二长岩常常被认为起源于富集地幔的熔融。本文报道了起源于增厚陆壳熔融的石英二长岩。雀莫错岩体是分布在羌塘北部(青藏高原中部)的雀莫错(湖)东北部雀莫山上的一个侵入体, 前人认为其由正长斑岩组成, 形成时代不确定(45~23 Ma)。近期, 我们对该侵入体进行了详细的野外地质调查和室内岩石学、地球化学以及年代学研究。雀莫错侵入岩主要由石英二长岩组成, 激光锆石 U-Pb 测年显示, 该岩体的侵位时代为始新世(41.71±0.29 Ma), 与区域上大面积始新世火山岩同期。雀莫错侵入岩高硅(SiO_2=65.12%~66.71%)、富碱(Na_2O+K_2O=9.08%~9.71%)、富钾(K_2O=5.50%~5.92%)和高铝(Al_2O_3>14.79%), 同时高 Sr (1874~2001 μg/g), 亏损重稀土 Yb (1.24~1.34 μg/g)和 Y (14.4~15.7 μg/g), 高 Sr/Y(124~136)和 La/Yb(67~74)比值, 富集大离子亲石元素(LILEs), 亏损高场强元素(HFSEs), 具有不明显的 Eu 负异常、Sr 正异常和略高的 $Mg^{\#}$(47~56), 与区域上大面积的同期埃达克质火山岩类似。岩石具有非常均一的($^{87}Sr/^{86}Sr)_i$ 同位素比值(~0.7069)和 $\varepsilon_{Nd}(t)$值(−2.6~ −2.8)。结合区域地质、岩石和构造资料, 认为雀莫错侵入岩形成于印度-欧亚大陆汇聚诱发的高原中部挤压阶段: 挤压导致陆内俯冲, 俯冲地壳发生部分熔融, 岩浆在上升的过程中与地幔橄榄岩发生小规模反应, 然后岩浆上升侵位形成了该区侵入岩。

关键词: 石英二长岩; 埃达克质岩石; 地壳增厚; 始新世; 羌塘; 青藏高原

中图分类号: P597; P595　　文献标志码: A　　文章编号: 1001-1552(2018)01-0150-013

0　引　言

富碱的中酸性岩石(如正长岩、石英二长岩)通常出现在伸展的背景下, 可以是后碰撞、裂谷或者板内环境(Yang et al., 2005, 2012; Wang et al., 2005a; Jung et al., 2007; Yang et al., 2007)。正长岩、石英二长岩出露的面积通常比较小, 但由于其形成的特殊构造背景受到广泛关注。正长岩、石英二长岩常富集碱、大离子亲石元素(LILEs)和轻稀土元素(LREEs), 亏损高场强元素(HREEs), 并具有相对富集的 Sr-Nd 同位素特征。关于其成因, 大多数学者认为其起源于富集地幔(Jung et al., 2005, 2007; Yang et al., 2005, 2012; Wang et al., 2005a; Jiang et al., 2006; He et al., 2009), 也有学者认为其可能起源于地壳岩

收稿日期: 2016-01-25; 改回日期: 2016-04-12

项目资助: 中国科学院前沿重点项目(QYZDJ-SSW-DQC026)、国家自然科学基金项目(41630208)、深地专项(2016YFC0600407)、广东人才项目(2014TX01Z079)和广州地化所"135"项目(135TP201601)联合资助。

第一作者简介: 曾纪鹏(1990–), 男, 硕士研究生, 岩石地球化学专业。

通信作者: 王强(1971–), 男, 研究员, 从事岩石学和地球化学研究。Email: wqiang@gig.ac.cn

石的部分熔融(Tchameni et al., 2001; Yang et al., 2012)。实验岩石学研究表明地壳岩石的高压熔融可以产生富碱的中酸性岩石(包括石英正长岩、石英二长岩)(Sen and Dunn, 1994; Skjerlie and Douce, 2002; Sisson et al., 2005)。因此, 石英正长岩、石英二长岩是否能够起源于地壳岩石的熔融, 还需要更多的实例来进一步检验。

青藏高原是世界上最大最高的高原, 拥有巨厚的地壳(60~90 km, Zhang et al., 2014)。但其地壳增厚的时间和机制一直是一个谜(Chung et al., 1998, 2003; Tapponnier et al., 2001; Wang et al., 2012)。一些研究从新生代埃达克岩的角度揭示, 青藏高原新生代地壳出现了明显的增厚: 如青藏高原中部羌塘地区始新世火山岩揭示该区在始新世发生了明显的地壳增厚并可能导致了高原隆升(Wang et al., 2008, 2010; Lai et al., 2013)。但是, 也有研究认为这些岩浆岩是拆沉下地壳熔融形成(Liu et al., 2003, 2008; Chen et al., 2013)。然而上述研究一直缺少同期侵入岩的证据。

雀莫错岩体为分布于青藏高原中部羌塘北部雀莫错(湖)东北部雀莫山上的一个侵入体。前人认为其由正长斑岩组成, 是近年来在 1∶25 万区域地质填图中新发现的, 但形成时代不确定(45~23 Ma)(白云山和李莉, 2002)。近期, 我们对该侵入岩进行了详细的野外地质调查和室内岩石学、地球化学以及年代学研究, 发现该侵入体由埃达克质石英二长岩组成并形成于始新世。开展该侵入岩研究对探讨石英二长岩的成因及其与高原地壳增厚之间的关系具有重要的意义。

1　地质背景与样品特征

青藏高原是由不同时期不同大陆块体拼贴形成的。从北到南, 青藏高原主要由近东西向的松潘-甘孜、羌塘和拉萨地块组成(Yin and Harrison, 2000; Chung et al., 2005)。它们之间的分界分别是金沙江、班公-怒江缝合带。通常认为, 松潘-甘孜与羌塘地块和羌塘与拉萨地块的缝合至少发生在白垩纪(Yin and Harrison, 2000), 白垩纪以来羌塘地块处于陆内构造背景(图 1)。

雀莫错位于羌塘地块的北部, 靠近金沙江缝合带。我们采集的样品位于雀莫错地区的雀莫山侵入体。岩体呈高耸近圆锥状山峰, 出露面积约为 22 km^2, 呈岩株状产出, 侵位于晚侏罗世雪山组碎屑岩中(白云山和李莉, 2002)。岩石为似斑状结构, 块状构造, 斑晶主要有钾长石(25%)、斜长石(15%)、黑云母(10%)、角闪石(8%)和石英(5%), 基质主要为钾长石、石英。钾长石具有明显的卡式双晶, 而斜长石中可见聚片双晶, 偶见环带。副矿物有锆石、磷灰石和 Fe-Ti 氧化物(图 2)。

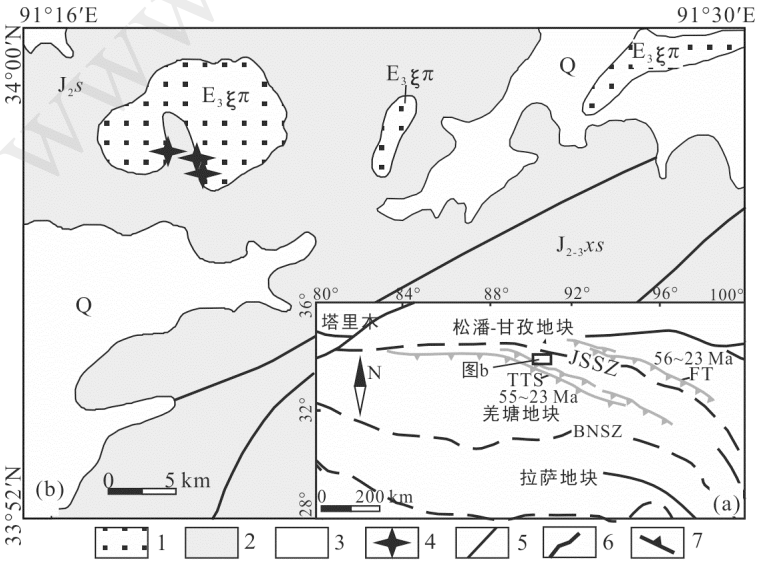

1. 始新世侵入岩; 2. 侏罗纪地层; 3. 第四纪地层; 4. 采样点; 5. 断层; 6. 逆冲断层; 7. 主要缝合带: JSSZ. 金沙江缝合带; BNSZ. 班公-怒江缝合带; TTS. 唐古拉山逆冲断层带; FT. 风火山逆冲断层带; 55~23 Ma: 逆冲断层带形成的时代(Li et al., 2015)。

图 **1**　青藏高原地质概图**(a**, 修改自 Li et al., 2015**)**和雀莫错区域地质简图**(b**, 修改自白云山和李莉, 2002**)**

Fig.1　Sketch map of the Tibetan Plateau (a) and regional geological map of the Qoimaco area (b)

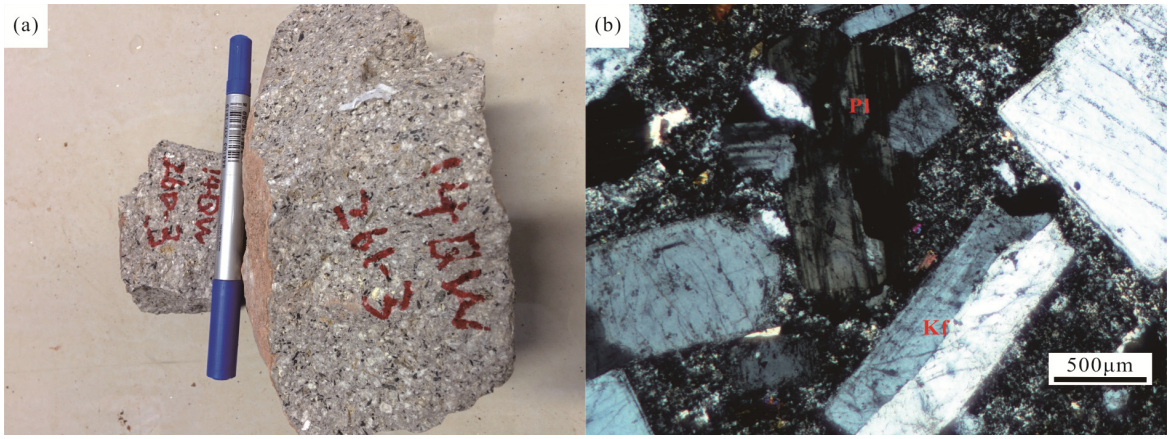

图 2 雀莫错石英二长岩手标本(a)和显微照片(b)(矿物名称缩写: Kf. 钾长石; Pl . 斜长石)

Fig.2 Hand specimen (a) and microphotograph (b) of the Qoimaco quartz-monzonite

2 分析方法

挑选新鲜的岩石样品, 人工碎至 3~5 mm, 用<5%的盐酸溶液和 Milli-Q 水反复清洗浸泡 3 次后烘干。之后在不锈钢钵中将样品粉碎至 200 目。主量、微量元素的分析测试均在中国科学院广州地球化学研究所同位素地球化学国家重点实验室完成。主量元素分析采用 Rigaku RIX 2000 型荧光光谱仪(XRF), 详细步骤见 Li et al. (2005), 分析精度优于 1%~5%。微量元素分析采用 Perkin-Elmer Sciex ELAN 6000 型电感耦合等离子体质谱仪(ICP-MS), 具体的流程见 Li (1997)。使用 USGS 标准 W-2 和 G-2 及国内标准 GSR-1、GSR-2 和 GSR-3 来校正所测样品的元素含量, 分析精度一般为 2%~5%。

Sr-Nd 同位素分析在中国科学院广州地球化学研究所同位素地球化学国家重点实验室完成, 所用仪器为 Micro Mass ISOPROBE 型多接收电感耦合等离子体质谱仪(MC-ICPMS)。采用 $HF+HNO_3$ 混合溶解样品, 用专用的阳离子交换柱进行分离。详细的分析测试流程及仪器分析情况见 Li et al. (2004)。所有测试的 $^{143}Nd/^{144}Nd$ 和 $^{87}Sr/^{86}Sr$ 比值分别用 $^{146}Nd/^{144}Nd=0.7219$ 和 $^{86}Sr/^{88}Sr=0.1194$ 校正。

使用浮选和电磁法进行锆石分选, 再在双目镜下挑选出晶形和透明度较好的锆石颗粒, 用无色透明的环氧树脂固定, 研磨抛光后进行显微照相。锆石阴极发光图像用 JXA-8100 电子探针完成。LA-ICP-MS 锆石 U-Pb 年龄测定在中国科学院地质与地球物理研究所岩石圈构造演化国家重点实验室完成, 所用仪器为激光剥蚀-Neptune 型多接收电感耦合等离子体质谱仪(LA-MC-ICPMS), 实验中 He 作为剥蚀物质的载气。用美国国家标准技术研究院研制的标准参考物质 NIST610 进行仪器最佳化, 采样方式为单点剥蚀。锆石 U-Pb 年龄测定采用国际标准锆石 91500 作为外标。数据处理采用 ICPMSDataCal 程序(Liu et al., 2010), 年龄计算及谐和图绘制用 Isoplot (ver 3.0) (Ludwig, 2003)完成。仪器的运行条件、详细分析流程见 Xie et al. (2008)。

3 分析结果

3.1 锆石 U-Pb 年代学

雀莫错侵入岩样品的锆石基本呈棱柱状, 粒径长度在 50~200 μm, 长宽比在 1∶1~4∶1 之间。锆石具有明显的环带结构, Th/U 比值均大于 0.4(表 1), 显示了典型的岩浆成因特征(图 3)。22 个有效测点的 $^{206}Pb/^{238}U$ 年龄在 40.4±0.6 Ma~43.4±1.0 Ma, 加权平均年龄为 41.71±0.29 Ma(n=22, MSWD=0.72)。所以, 我们认为雀莫错侵入岩的侵位时代为始新世(~42 Ma)。

3.2 主量、微量元素

雀莫错侵入岩的主量、微量元素分析结果见表 2。岩石具有高 SiO_2(65.12%~66.71%), 为酸性侵入岩。岩石具有高的全碱含量(Na_2O+K_2O=9.08%~9.71%), 在 TAS 图解(图 4a)上, 落入石英二长岩区域内, 与同期的多格错仁和祖尔肯乌拉山火山岩相比, 具有相对较高的碱含量。岩石也具有高的 K_2O 含量(5.50%~5.92%), 在 SiO_2-K_2O 图中(图 4b), 样品主要落入钾玄质系列区域, 比同期的火山岩具有较高的 K_2O 含量。同时, 样品含有较高的 Al_2O_3 含量(≥14.79%), 铝饱和指数 A/CNK 为 0.87~0.91, 在 A/CNK-A/NK 图解(图 5b)中, 样品落在准铝质区域, 与同期火山岩一致。岩石的 MgO 含量为 1.47%~2.31%, $Mg^{\#}$ 较高为 47~56。

表 1　雀莫错石英二长岩 LA-ICP-MS 锆石 U-Pb 定年结果

Table 1　LA-ICP-MS U-Pb dating results of zircons from the Qoimaco quartz-monzonite

分析点	含量(μg/g)		Th/U	同位素比值						年龄(Ma)	
	Th	U		$^{207}Pb/^{206}Pb$	1σ	$^{207}Pb/^{235}U$	1σ	$^{206}Pb/^{238}U$	1σ	$^{206}Pb/^{238}U$	1σ
14QW263-1-1	251	411	0.61	0.0490	0.0037	0.0422	0.0030	0.0064	0.0001	40.9	0.8
14QW263-1-2	1082	1452	0.75	0.0476	0.0019	0.0426	0.0018	0.0064	0.0001	41.4	0.6
14QW263-1-3	1230	1412	0.87	0.0505	0.0022	0.0447	0.0019	0.0065	0.0001	41.8	0.6
14QW263-1-4	1254	1509	0.83	0.0495	0.0024	0.0425	0.0020	0.0063	0.0001	40.4	0.6
14QW263-1-5	691	652	1.06	0.0490	0.0032	0.0417	0.0027	0.0064	0.0002	41	0.9
14QW263-1-6	509	486	1.05	0.0485	0.0037	0.0439	0.0034	0.0068	0.0002	43.4	1.0
14QW263-1-7	1257	1653	0.76	0.0478	0.0029	0.0414	0.0024	0.0063	0.0001	40.8	0.9
14QW263-1-8	1276	1487	0.86	0.0488	0.0020	0.0418	0.0017	0.0063	0.0001	40.6	0.8
14QW263-1-9	2084	1896	1.10	0.0466	0.0020	0.0425	0.0018	0.0066	0.0001	42.1	0.7
14QW263-1-10	1509	1712	0.88	0.0494	0.0017	0.0436	0.0015	0.0064	0.0001	41.2	0.6
14QW263-1-11	516	568	0.91	0.0491	0.0033	0.0419	0.0027	0.0064	0.0002	41.4	1
14QW263-1-12	1205	1216	0.99	0.0474	0.0024	0.0415	0.0021	0.0064	0.0001	40.9	0.6
14QW263-1-13	1131	1060	1.07	0.0498	0.0024	0.0440	0.0021	0.0065	0.0001	41.6	0.7
14QW263-1-14	1078	958	1.13	0.0479	0.0030	0.0433	0.0025	0.0067	0.0001	43.0	0.8
14QW263-1-15	1242	1191	1.04	0.0453	0.0023	0.0402	0.0018	0.0066	0.0001	42.4	0.7
14QW263-1-16	811	1116	0.73	0.0508	0.0025	0.0439	0.0020	0.0064	0.0001	40.9	0.6
14QW263-1-17	1274	1693	0.75	0.0498	0.0017	0.0436	0.0014	0.0064	0.0001	41.1	0.6
14QW263-1-18	725	995	0.73	0.0477	0.0023	0.0426	0.0022	0.0064	0.0001	41.4	0.7
14QW263-1-19	889	980	0.91	0.0479	0.0026	0.0412	0.0021	0.0063	0.0001	40.7	0.7
14QW263-1-20	1490	1636	0.91	0.0510	0.0024	0.0446	0.0019	0.0064	0.0001	41.3	0.6
14QW263-1-21	1456	942	1.55	0.0496	0.0023	0.0438	0.0019	0.0065	0.0001	41.7	0.6
14QW263-1-22	1368	1627	0.84	0.0487	0.0018	0.0429	0.0014	0.0065	0.0001	41.6	0.6

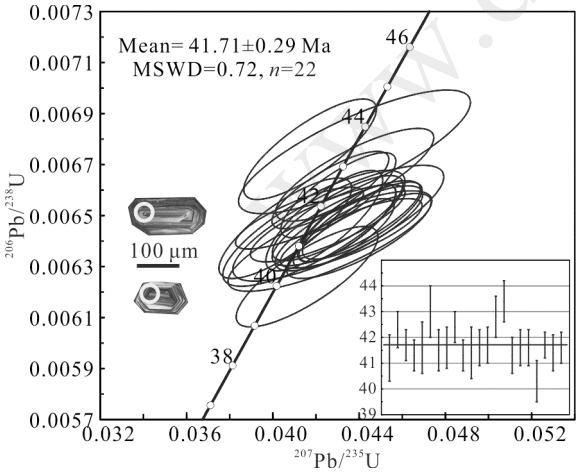

图 3　样品 14QW263-1 锆石 U-Pb 年龄谐和图

Fig.3　U-Pb concordia diagram of zircons from the quartz-monzonite

雀莫错侵入岩稀土元素的总量(∑REE)介于 336.10~388.82 μg/g 之间。在球粒陨石标准化稀土元素配分模式图上(图 6a), 稀土元素配分曲线呈一致的右倾型, 轻重稀土元素之间的分馏非常明显(La/Yb=67~74), 且轻稀土元素的分异程度(La/Sm=8.4~9.0)大于重稀土元素(Gd/Yb=5.4~5.6), 具有不明显的 Eu 负异常(δEu=0.85~0.87)。在原始地幔标准化微量元素蛛网图中(图 6b), 样品富集 LILEs(Ba、Sr 和 Pb 等), 明显亏损 HFSEs(Nb、Ta 和 Ti 负异常), 低 Y 和 Yb 含量, 高 Sr/Y 比值(124~136)和不明显的 Sr 正异常。

3.3　Sr-Nd 同位素

样品具有非常均一的初始($^{87}Sr/^{86}Sr)_i$ 同位素比值(0.7069)和 $\varepsilon_{Nd}(t)$值(−2.6~−2.8), 落在同时代埃达克质岩石范围内, 其两阶段模式年龄(t_{DM2})为 0.84~0.86 Ga (表 2, 图 7)。

4　讨　论

4.1　北羌塘地块始新世岩浆作用及构造背景

本文新的锆石 U-Pb 年龄以及现今已发表的高精度年龄数据(Roger et al., 2000; Lai et al., 2003, 2013; Spurlin et al., 2005; Guo et al., 2006; Jiang et al., 2006; Liu et al., 2008; 董彦辉等, 2008; Wang et al., 2008, 2010; Chen et al., 2013; Long et al., 2015)表明,

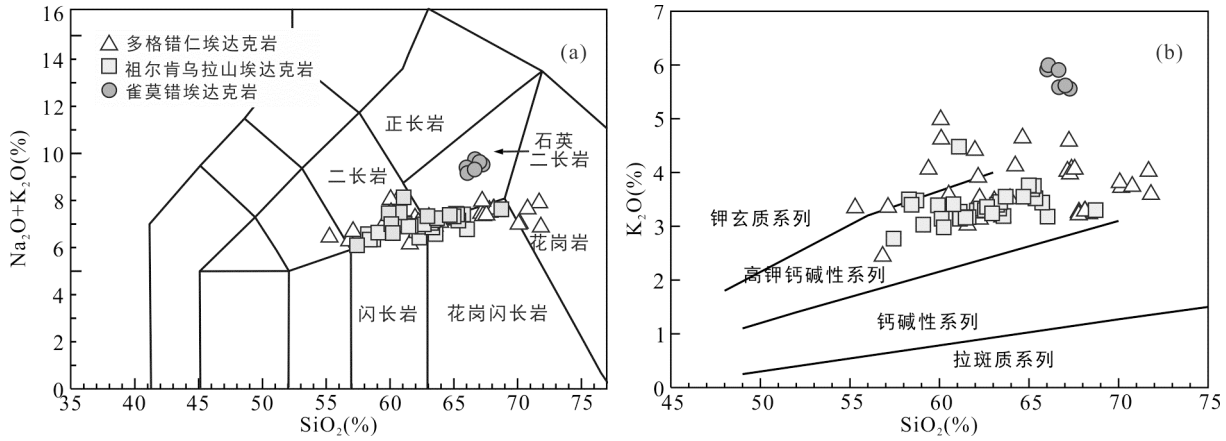

多格错仁埃达克岩和祖尔肯乌拉山埃达克岩数据分别来自 Wang et al. (2008)和 Lai et al. (2013)。

图 4 **TAS (a**, Middlemost, 1994)和 **SiO_2-K_2O (b**, Peccerillo and Taylor, 1976)图解

Fig.4 Plots of SiO_2 *vs.* K_2O+Na_2O (a) and SiO_2 *vs.* K_2O (b)

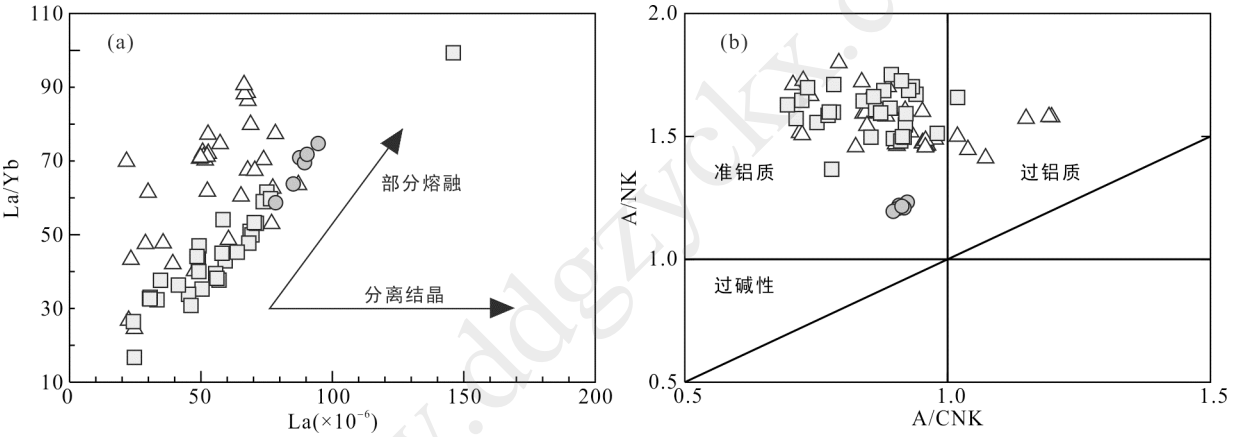

图 5 雀莫错石英二长岩 **La-La/Yb (a)**和 **A/CNK-A/NK (b**, Maniar and Piccoli, 1989)图解(图例及数据来源同图 3)

Fig.5 La *vs.* La/Yb (a) and A/CNK *vs.* A/NK (b) diagrams for the Qoimaco quartz-monzonites

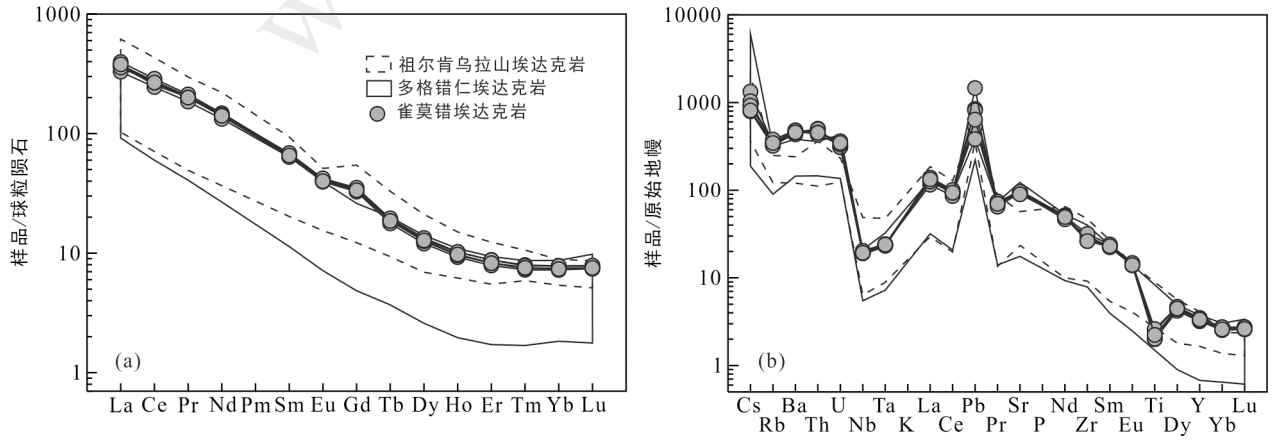

图 6 雀莫错石英二长岩球粒陨石标准化稀土元素配分模式图**(a)**和原始地幔标准化微量元素蛛网图**(b)**(数据来源同图 3, 球粒陨石和原始地幔标准化值引自 Sun and McDonough, 1989)

Fig.6 Chondrite-normalized REE patterns (a), and primitive mantle-normalized trace element spider diagram (b) of the Qoimaco quartz-monzonites

表 2　雀莫错石英二长岩主量(%)、微量(μg/g)元素和 Sr-Nd 同位素分析结果

Table 2　Major (%), trace element (μg/g) concetrations and Sr-Nd isotopic compositions for the Qoimaco quartz-monzonites

样号	14QW261-1	14QW261-2	14QW261-3	14QW262	14QW263-1	14QW263-2
SiO_2	66.71	66.24	66.68	65.12	65.30	65.21
TiO_2	0.45	0.45	0.45	0.52	0.58	0.48
Al_2O_3	15.04	15.38	15.40	15.02	14.79	14.93
Fe_2O_3*	3.34	3.33	3.24	3.59	3.53	3.10
MnO	0.12	0.11	0.12	0.12	0.10	0.10
MgO	1.56	1.58	1.47	2.06	2.31	1.66
CaO	2.29	2.35	2.30	2.61	2.78	2.94
Na_2O	3.97	4.17	4.03	3.48	3.16	3.36
K_2O	5.50	5.54	5.58	5.84	5.92	5.77
P_2O_5	0.20	0.21	0.21	0.31	0.35	0.30
LOI	0.34	0.35	0.47	0.73	1.09	1.53
Total	99.52	99.72	99.96	99.40	99.93	99.38
$Mg^{\#}$	48.1	48.5	47.4	53.2	56.5	51.5
Sc	5.19	5.45	5.32	6.74	6.84	5.93
V	43.3	44.5	42.8	52.4	55.5	47.1
Cr	45.2	48.4	37.4	60.0	55.0	51.9
Co	6.52	6.56	6.02	8.82	8.60	6.76
Ni	27.7	28.4	27.3	36.2	36.6	28.8
Cu	10.8	7.40	8.19	32.8	53.3	10.70
Zn	75.3	58.7	74.5	109	90.9	60.8
Ga	19.8	20.1	20.0	19.7	19.4	19.4
Ge	2.56	2.61	2.51	2.55	2.61	2.44
Rb	211	204	202	219	237	217
Sr	1964	1985	1986	1957	2001	1874
Y	14.4	15.0	14.9	15.7	15.7	15.1
Zr	293	292	292	336	352	291
Nb	13.7	13.4	13.5	13.9	14.4	13.6
Cs	10.4	8.09	6.19	7.16	7.23	6.35
Ba	2994	3212	3124	3333	3312	3160
La	87.59	89.43	94.61	78.43	85.12	90.37
Ce	165.50	169.30	176.90	150.80	163.50	164.30
Pr	19.15	19.60	20.31	17.70	19.16	19.13
Nd	65.69	67.59	69.47	62.33	67.35	66.19
Sm	9.93	10.24	10.48	9.82	10.57	10.01
Eu	2.31	2.40	2.41	2.32	2.46	2.33
Gd	6.75	7.03	7.11	6.87	7.27	6.94
Tb	0.67	0.70	0.71	0.72	0.73	0.70
Dy	3.07	3.22	3.24	3.33	3.42	3.26
Ho	0.53	0.55	0.55	0.58	0.58	0.56
Er	1.31	1.37	1.38	1.46	1.46	1.37
Tm	0.19	0.19	0.20	0.20	0.20	0.19
Yb	1.24	1.29	1.27	1.34	1.34	1.26
Lu	0.19	0.19	0.19	0.20	0.20	0.19
Hf	8.14	8.04	8.17	9.13	9.68	8.05
Ta	0.938	0.936	0.955	0.970	0.979	0.963
Pb	59.3	37.2	57.1	102	44.7	26.9
Th	42.3	41.4	41.7	35.9	38.2	37.9
U	6.42	6.60	6.44	6.89	7.50	7.19
∑REE	364.11	373.10	388.82	336.10	363.37	366.86
δEu	0.86	0.86	0.85	0.87	0.86	0.85
$^{87}Sr/^{86}Sr$	0.707111±15		0.707103±18		0.707105±16	
$(^{87}Sr/^{86}Sr)_i$	0.706934		0.706936		0.706910	
$^{143}Nd/^{144}Nd$	0.512473±11		0.512465±12		0.512476±11	
$^{143}Nd/^{144}Nd(t)$	0.512449		0.512441		0.512451	
$\varepsilon_{Nd}(t)$	2.68		−2.84		−2.64	
t_{DM2}(Ga)	0.84		0.85		0.86	

注: Fe_2O_3*. 全铁; LOI. 烧失量; $Mg^{\#}=Mg^{2+}/(Fe^{2+}+Mg^{2+})\times100$; $\delta Eu=Eu_N/(Sm_N\times Gd_N)^{1/2}$; Sr、Nd 同位素初始值按 t=40 Ma 为回算年龄。

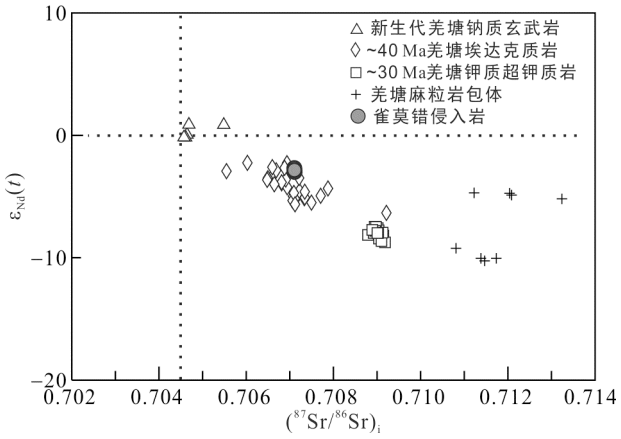

羌塘新生代~60 Ma 钠质玄武岩数据来自 Ding et al. (2003)和邓万明等(2001); ~40 Ma 羌塘埃达克质岩数据来自 Wang et al. (2008)和 Lai et al. (2013); ~30 Ma 羌塘钾质超钾质岩数据来自 Ding et al. (2003); 羌塘麻粒岩包体数据来自 Lai et al. (2011)。

图 7 雀莫错石英二长岩($^{87}Sr/^{86}Sr)_i$-$\varepsilon_{Nd}(t)$同位素图解

Fig.7 Sr *vs.* Nd isotope diagram for the Qoimaco quartz-monzonites

始新世可能是北羌塘地块岩浆活动的高峰期。该时期出露的岩石主要为中酸性埃达克质火山岩，岩石类型有流纹岩、安山岩、英安岩、粗面岩和粗安岩等，以及少量的橄榄玄粗岩。而岩石的分布从多格错仁地区、枕头崖-祖尔肯乌拉山、唐古拉山到玉树-囊谦地区以及玉龙地区，大体与缝合线一致呈近东西向带状展布(Wang et al., 2008, 2010)。

前人研究(郑祥身和郑健康，1997; 白云山和李莉，2002)认为雀莫错侵入岩是在青藏高原经历南北向挤压缩短的过程中，在羌塘地块上自南向北产生的平行于主压应力方向的张性构造，导致了岩浆沿该张性构造产出。最近的资料显示，在羌塘地块北部和松潘-甘孜南部，变形作用和可可西里盆地的连续填充显示唐古拉山逆冲断层带(TTS)和风火山-囊谦逆冲断层带(FT)在始新世-渐新世经历了强烈的地壳缩短(Wang et al., 2002; Spurlin et al., 2005; Li et al., 2015)，并且在 23 Ma 之前结束(Wang et al., 2002; Wu et al., 2008; Li et al., 2015)。广泛分布的新生代碎屑岩在该时期沉积了下来，这也是对该地区始新世-渐新世强烈变形、地壳增厚以及剥蚀的一种响应(Ding et al., 2000; Lai et al., 2001)。所以，我们认为雀莫错侵入岩形成于挤压的构造背景。

4.2 雀莫错侵入岩的成因

雀莫错侵入岩具有明显的埃达克质岩的地球化学特征，如高 SiO_2(>56%)、Al_2O_3(>14.8%)含量，高 Sr 含量(>1500 μg/g)、低 HREEs(如 Yb<1.40 μg/g)和 Y(<16.0 μg/g)以及高 Sr/Y(>100)比值。轻重稀土元素分异明显，不明显 Eu 和 Sr 异常，在 Y-Sr/Y 图解(图 8a)中落在埃达克岩的范围内。

关于埃达克质岩石的成因，有多种解释：(1)热的年轻的洋壳熔融(Defant and Drummond, 1990); (2)玄武质岩浆的分离结晶作用(Castillo et al., 1999; Macpherson et al., 2006); (3)酸性岩浆与玄武质岩浆的混合作用(Streck et al., 2007); (4)拆沉下地壳部分熔融(Xu et al., 2002; Gao et al., 2004; Wang et al., 2006b); (5)增厚下地壳部分熔融(Atherton and Petford, 1993; Chung et al., 2003; Wang et al., 2005b)。

通常来讲，洋壳部分熔融产生的埃达克质岩富 Na_2O、贫 K_2O，具有低的 K_2O/Na_2O 比值(≤0.4) (Defant and Drummond, 1990)。而雀莫错侵入岩具有高的 K_2O 含量(5.50%~5.92%)和 K_2O/Na_2O 比值(>1.3)。

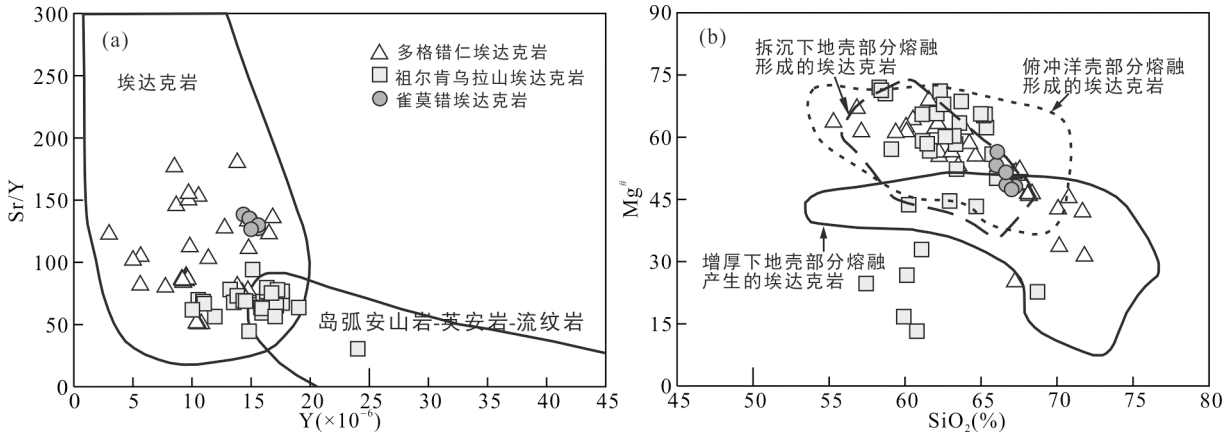

图 **8** 雀莫错石英二长岩 **Y-Sr/Y** 图解(**a**，据 Defant and Drummond, 1990)和 **SiO_2-$Mg^{\#}$**图解(**b**，据 Wang et al., 2006b)(数据来源同图 3)

Fig.8 Y *vs.* Sr/Y (a) and SiO_2 *vs.* $Mg^{\#}$ (b) diagrams for the Qoimaco quartz-monzonites

并且, 自中侏罗世以来, 羌塘进入了陆内背景。因此, 雀莫错侵入岩不可能是洋壳部分熔融形成的。通过玄武质岩浆的分离结晶作用形成的埃达克岩通常会有较宽的 SiO_2 范围, 在 Hacker 图解中会有线性的变化趋势, 而雀莫错侵入岩具有非常均一的地球化学成分, 并且在 La/Yb-La 图解(图 5a)中也显示部分熔融的趋势, 而非分离结晶。再者, 分离结晶形成如此面积的中酸性岩浆需要比这大很多的母源基性岩浆存在, 而侵入岩附近并没有同时代的基性岩浆出露。岩浆混合产生的岩石会在一些二元图解中显示一定的线性关系(Macpherson et al., 2006), 但在 K_2O、Al_2O_3、La、Rb 与 SiO_2 的图解中并未显示出这样的关系。并且雀莫错侵入岩高的 SiO_2 含量以及不存在基性的包体表明其可能不是由酸性岩浆与玄武质岩浆混合形成的。

拆沉下地壳来源的埃达克质岩石通常形成于伸展背景(Gao et al., 2004; Liu et al., 2008; Chen et al., 2013), 而本文研究的岩石形成于挤压环境。另外, 来自北羌塘地区的捕掳体成分表明, 羌塘下地壳主要是早中生代或者新生代俯冲下来的松潘-甘孜三叠纪沉积岩(Hacker et al., 2000, 2005; Yin and Harrison, 2000; Kapp et al., 2003, 2005), 并且在相同的温压条件下, 其密度低于地幔岩石而不易于拆沉(Hacker et al., 2005; Wang et al., 2008)。

增厚下地壳来源的埃达克质岩石通常具有较低的 $Mg^{\#}$、Cr 和 Ni 含量(Wang et al., 2005b, 2008; Long et al., 2015), 而雀莫错侵入岩具有较高的 $Mg^{\#}$、Cr 和 Ni 含量, 这说明岩石的形成过程中有地幔组分的贡献。在 Sr-Nd 同位素图解上(图 7), 雀莫错侵入岩落在同时代埃达克质火山岩的区域内, 并且他们还具有相似的稀土和微量元素分布, 表明他们可能来自相同的源区。羌塘这些始新世埃达克质火山岩中, 一些准铝质-高 $Mg^{\#}$埃达克质岩石被认为是新生代向南俯冲的松潘-甘孜以沉积物为主的陆壳熔体与地幔橄榄岩反应而形成的(Wang et al., 2008, 2010)。雀莫错侵入岩具有准铝质-高 $Mg^{\#}$特征(图 5b、8b), 高 Th/La 比值(0.42~0.48)与羌塘准铝质-高 $Mg^{\#}$埃达克质火山岩 Th/La 比值(0.21~0.71, Wang et al., 2008)类似, 但其 Th 含量(35.9~42.3 μg/g)比羌塘准铝质-高 $Mg^{\#}$埃达克质火山岩的 Th 含量(12.3~30.4 μg/g)更高。因此, 我们认为雀莫错准铝质-高 $Mg^{\#}$埃达克质侵入岩的成因类似于羌塘准铝质-高 $Mg^{\#}$埃达克质火山岩, 是由向南俯冲的松潘-甘孜地块以沉积物为主的陆壳熔体与地幔橄榄岩反应而形成的(Wang et al., 2008, 2010), 但其源区可能包含了更多的沉积物组分。另外, 雀莫错准铝质-高 $Mg^{\#}$埃达克质侵入岩无 Eu 异常、Sr 正异常、强烈亏损 HREEs 和 Nb、Ta, 说明岩浆来源于石榴石+金红石稳定源区, 且几乎不含斜长石(Rapp et al., 1999, 2003; Xiong et al., 2005)。实验岩石学研究表明, 含石榴石+金红石残留矿物且几乎不含斜长石的岩浆源区深度>50 km (Rapp et al., 1999, 2003; Xiong et al., 2005; Wang et al., 2008; Ma et al., 2014), 暗示该区在始新世(~42 Ma)已经发生了明显地壳增厚。

4.3　动力学过程及意义

自~55 Ma 印度-欧亚大陆碰撞以来, 印度岩石圈仍以一定的速度向北俯冲, 持续挤压使得金沙江缝合带重新活动(Yin and Harrison, 2000; Tapponnier et al., 2001)。考虑到始新世高原中部发生了明显地壳缩短(Wang et al., 2002; Spurlin et al., 2005; Li et al., 2015)以及羌塘北部呈近东西向带状分布的大量岩浆岩及其成因(Ding et al., 2007; Wang et al., 2008, 2010; Lai et al., 2013), 我们认为在新生代由于印度-欧亚板块南北汇聚导致挤压, 松潘-甘孜地块沿着金沙江缝合带南向俯冲。地球物理资料显示, 松潘-甘孜地块已经俯冲到羌塘地块之下(Kind et al., 2002; Zhao et al., 2011)。松潘-甘孜地块主要是由沉积物和早期的玄武岩层组成, 随着松潘-甘孜地块的俯冲, 玄武岩层在榴辉岩相条件下开始脱水, 而沉积物在高压下具有相对低的固相线(Johnson and Plank, 1999), 上升流体引起了沉积物为主的陆壳的熔融, 产生了原始埃达克质熔体, 上升过程中与地幔橄榄岩反应形成了雀莫错侵入岩(Wang et al., 2008)。

Wang et al. (2008)和 Long et al. (2015)在羌塘北部报道了形成于加厚下地壳的始新世埃达克质岩石, 暗示当时在羌塘北部已经处于增厚的状态, 并且高原已经开始隆升了。本次报道的始新世雀莫错埃达克质岩石的形成与陆内俯冲有关, 俯冲过程导致地壳挤压增厚。因此, 青藏高原地壳增厚很可能是印度岩石圈持续北向俯冲以及松潘-甘孜地块南向俯冲共同作用的结果。在新生代, 陆壳俯冲可能是青藏高原巨厚地壳形成的重要机制。

5　结　论

综上所述, 羌塘雀莫错地区侵入岩由石英二长岩组成, 形成于~42 Ma, 具有埃达克质岩石的地球化学特征。该侵入岩形成于印度-欧亚大陆汇聚诱

发的高原中部挤压阶段: 挤压导致陆内俯冲, 俯冲地壳发生部分熔融, 岩浆在上升过程中与地幔橄榄岩反应, 岩浆上升侵位形成了雀莫错侵入岩。在新生代, 陆壳俯冲可能是青藏高原巨厚地壳形成的重要机制。

致谢: 在室内样品处理和化学分析以及论文撰写过程中得到了涂湘林、胡光黔、曾文、孙胜玲等老师和王鑫玉博士的帮助和指导, 西北大学龙晓平教授和另一位匿名审稿专家对文章提出的宝贵修改意见, 在此一并表示感谢。

参考文献(References):

白云山, 李莉. 2002. 羌塘中部雀莫正长斑岩体特征及构造意义. 岩石矿物学杂志, 21(2): 169–173.

邓万明. 2001. 西羌塘第三纪钠质基性火山岩的地球化学特征及成因探讨. 中国科学(D辑), 31(B12): 43–54.

邓万明, 孙宏娟, 张玉泉. 2001. 囊谦盆地新生代钾质火山岩成因岩石学研究. 地质科学, 36(3): 304–318.

董彦辉, 王强, 许继峰, 资锋. 2008. 羌塘地块北部东月湖始新世高$Mg^{\#}$埃达克质火山岩的成因以及构造意义. 岩石学报, 24(2): 291–302.

郑祥身, 郑健康. 1997. 青海可可西里地区侵人岩的岩石化学特征及其成因意义研究. 岩石学报, 13(1): 44–58.

Atherton M P and Petford N. 1993. Generation of sodium-rich magmas from newly underplated basaltic crust. *Nature*, 362: 144–146.

Castillo P R, Janney P E and Solidum R U. 1999. Petrology and geochemistry of Camiguin Island, southern Philippines: Insights to the source of adakites and other lavas in a complex arc setting. *Contributions to Mineralogy and Petrology*, 134: 33–51.

Chen J L, Wu J B, Xu J F, Dong Y F, Wang B D and Kang Z Q. 2013. Geochemistry of Eocene high-Mg# adakitic rocks in the northern Qiangtang terrane, central Tibet: Implications for early uplift of the plateau. *Geological Society of America Bulletin*, 125(11–12): 1800–1819.

Chung S L, Chu M F, Zhang Y, Xie Y, Lo C H, Lee T Y, Lan C Y, Li X, Zhang Q and Wang Y. 2005. Tibetan tectonic evolution inferred from spatial and temporal variations in post-collisional magmatism. *Earth-Science Reviews*, 68 (3–4): 173–196.

Chung S L, Liu D Y, Ji J Q, Chu M F, Lee H Y, Wen D J, Lo C H, Lee T Y, Qian Q and Zhang Q. 2003. Adakites from continental collision zones: Melting of thickened lower crust beneath southern Tibet. *Geology*, 31: 1021–1024.

Chung S L, Lo C H, Lee T Y, Zhang Y, Xie Y, Li X, Wang K L and Wang P L. 1998. Diachronous uplift of the Tibetan plateau starting 40 Myr ago. *Nature*, 394(6695): 769–773.

Defant M J and Drummond M S. 1990. Derivation of some modern arc magmas by melting of young subducted lithosphere. *Nature*, 347(6294): 662–665.

Ding L, Kapp P, Yue Y and Lai Q. 2007. Postcollisional calc-alkaline lavas and xenoliths from the southern Qiangtang terrane, central Tibet. *Earth and Planetary Science Letters*, 254(1): 28–38.

Ding L, Kapp P, Zhong D L and Deng W M. 2003. Cenozoic volcanism in Tibet: Evidence for a transition from oceanic to continental subduction. *Journal of Petrology*, 44: 1833–1865.

Ding L, Zhou Y, Zhang J J and Deng W M. 2000. Geologic relationships and geochronology of the Cenozoic volcanoes and interbedded weathered mantles of Yulinshan in Qiangtang, North Tibet. *Chinese Science Bulletin*, 45(24): 2214–2220.

Gao S, Rudnick R L, Yuan H L, Liu X M, Liu Y S, Xu W L, Ling W L, Ayers J, Wang X C and Wang Q H. 2004. Recycling lower continental crust in the north china craton. *Nature*, 432(7019): 892–897.

Guo Z F, Wilson M, Liu J Q and Mao Q. 2006. Post-collisional, potassic and ultrapotassic magmatism of the northern Tibetan Plateau: Constraints on characteristics of the mantle source, geodynamic setting and uplift mechanisms. *Journal of Petrology*, 47(6): 1177–1220.

Hacker B R, Gnos E, Ratschbacher L, Grove M, McWilliams M, Sobolev S V, Wan J and Wu Z H. 2000. Hot and dry deep crustal xenoliths from Tibet. *Science*, 287(5462): 2463–2466.

Hacker B R, Luffi P, Lutkov V, Minaev V, Ratschbacher L, Plank T, Ducea M, Patiño Dounce A, McWilliams M and Metcalf J. 2005. Near-ultrahigh pressure processing of continental crust: Miocene crustal xenoliths from the Pamir. *Journal of Petrology*, 46(8): 1661–1687.

He Z Y, Xu X S, Yao Y and Zou H B. 2009. Origin of the Late Cretaceous syenite from Yandangshan, SE China, constrained by zircon U-Pb and Hf isotopes and geochemical data. *International Geology Review*, 51(6): 556–582.

Jiang Y H, Jiang S Y, Ling H F and Dai B Z. 2006.

Low-degree melting of a metasomatized lithospheric mantle for the origin of Cenozoic Yulong monzogranite-porphyry, east Tibet: Geochemical and Sr-Nd-Pb-Hf isotopic constraints. *Earth and Planetary Science Letters*, 241(3): 617–633.

Johnson M C and Plank T. 1999. Dehydration and melting experiments constrain the fate of subducted sediments. *Geochemistry*, *Geophysics*, *Geosystems*, 1(12). DOI: 10.1029/1999GC000014

Jung S, Hoernes S and Hoffer E. 2005. Petrogenesis of cogenetic nepheline and quartz syenites and granites (Northern Damara Orogen, Namibia): Enriched mantle versus crustal contamination. *The Journal of Geology*, 113(6): 651–672.

Jung S, Hoffer E and Hoernes S. 2007. Neo-Proterozoic rift-related syenites (Northern Damara Belt, Namibia): Geochemical and Nd-Sr-Pb-O isotope constraints for mantle sources and petrogenesis. *Lithos*, 96(3): 415–435.

Kapp P, Murphy M A, Yin A, Harrison T M, Ding L and Guo J. 2003. Mesozoic and Cenozoic tectonic evolution of the Shiquanhe area of western Tibet. *Tectonics*, 22(4). DOI: 10.1029/2001TC001332

Kapp P, Yin A, Harrison T M and Ding L. 2005. Cretaceous-Tertiary shortening, basin development, and volcanism in central Tibet. *Geological Society of America Bulletin*, 117: 865–878.

Kind R, Yuan X, Saul J, Nelson D, Sobolev S V, Mechie J, Zhao W J, Kosarev G, Ni J, Achauer U and Jiang M. 2002. Seismic images of crust and upper mantle beneath Tibet: Evidence for Eurasian plate subduction. *Science*, 298(5596): 1219–1221.

Lai S C, Liu C Y and O'Reilly S Y. 2001. Petrogenesis and its significance to continental dynamics of the Neogene high-potassium calc-alkaline volcanic rock association from north Qiangtang, Tibetan Plateau. *Science in China Series D*: *Earth Sciences*, 44(1): 45–55.

Lai S C and Qin J F. 2013. Adakitic rocks derived from the partial melting of subducted continental crust: Evidence from the Eocene volcanic rocks in the northern Qiangtang block. *Gondwana Research*, 23(2): 812–824.

Lai S C, Qin J F and Grapes R. 2011. Petrochemistry of granulite xenoliths from the Cenozoic Qiangtang volcanic field, northern Tibetan plateau: Implications for lower crust composition and genesis of the volcanism. *International Geology Review*, 53(8): 926–945.

Li X H. 1997. Geochemistry of the Longsheng Ophiolite from the southern margin of Yangtze Craton, SE China. *Geochemical Journal*, 31(5): 323–337.

Li X H, Liu D Y, Sun M, Li W X, Liang X R and Liu Y. 2004. Precise Sm-Nd and U-Pb isotopic dating of the supergiant Shizhuyuan polymetallic deposit and its host granite, SE China. *Geological Magazine,* 141: 225–231.

Li X H, Qi C S, Liu Y, Liang X R, Tu X L, Xie L W and Yang Y H. 2005. Petrogenesis of the Neoproterozoic bimodal volcanic rocks along the western margin of the Yangtze Block: New constraints from Hf isotopes and Fe/Mn ratios. *Chinese Science Bulletin*, 50(21): 2481–2486.

Li Y L, Wang C S, Dai J G, Xu G Q, Hou Y L and Li X H. 2015. Propagation of the deformation and growth of the Tibetan–Himalayan orogen: A review. *Earth-Science Reviews*, 143: 36–61.

Liu S, Hu R Z, Feng C X, Zou H B, Li C, Chi X G, Peng J T, Zhong H, Qi L, Qi Y Q and Wang T. 2008. Cenozoic high Sr/Y volcanic rocks in the Qiangtang terrane, northern Tibet: Geochemical and isotopic evidence for the origin of delaminated lower continental melts. *Geological Magazine*, 145(4): 463–474.

Liu Y S, Gao S, Hu Z C, Gao C G, Zong K Q and Wang D B. 2010. Continental and oceanic crust recycling-induced melt-peridotite interactions in the Trans-North China Orogen: U-Pb dating, Hf isotopes and trace elements in zircons from mantle xenoliths. *Journal of Petrology*, 51(1–2): 537–571.

Long X P, Wilde S A, Wang Q, Yuan C, Wang X C, Li J, Jiang Z Q and Dan W. 2015. Partial melting of thickened continental crust in central Tibet: Evidence from geochemistry and geochronology of Eocene adakitic rhyolites in the northern Qiangtang Terrane. *Earth and Planetary Science Letters*, 414: 30–44.

Ludwig K R. 2003. User's manual for Isoplot 3.00: A geochronological toolkit for Microsoft Excel. Berkeley Geochronology Center Special Publication, 4: 1–70

Ma L, Wang B D, Jiang Z Q, Wang Q, Li Z X, Wyman D A, Zhao S R, Yang J H, Gou G N and Guo H F. 2014. Petrogenesis of the Early Eocene adakitic rocks in the Napuri area, southern Lhasa: Partial melting of thickened lower crust during slab break-off and implications for crustal thickening in southern Tibet. *Lithos*, 196:

321–338.

Macpherson C G, Dreher S T and Thirlwall M F. 2006. Adakites without slab melting: High pressure differentiation of island arc magma, Mindanao, the Philippines. *Earth and Planetary Science Letters*, 243: 581–593.

Maniar P D and Piccoli P M. 1989. Tectonic discrimination of granitoids. *Geological Society of America Bulletin*, 101(5): 635–643.

Middlemost E A K. 1994. Naming materials in the magma/igneous rock system. *Earth-Science Reviews*, 37(3): 215–224.

Peccerillo A and Taylor S R. 1976. Geochemistry of Eocene calc-alkaline volcanic rocks from the Kastamonu area, northern Turkey. *Contributions to Mineralogy and Petrology*, 58(1): 63–81.

Rapp R P, Shimizu N and Norman M D. 2003. Growth of early continental crust by partial melting of eclogite. *Nature*, 425(6958): 605–609.

Rapp R P, Shimizu N, Norman M D and Applegate G S. 1999. Reaction between slab-derived melts and peridotite in the mantle wedge: Experimental constraints at 3.8 GPa. *Chemical Geology*, 160: 335–356.

Roger F, Tapponnier P, Arnaud N, SchaÈrer U, Brunel M, Zhiqin X and Jingsui Y. 2000. An Eocene magmatic belt across central Tibet: Mantle subduction triggered by the Indian collision? *Terra Nova*, 12(3): 102–108.

Sen C and Dunn T. 1994. Dehydration melting of a basaltic composition amphibolite at 1.5 and 2.0 GPa: Implications for the origin of adakites. *Contributions to Mineralogy and Petrology*, 117(4): 394–409.

Sisson T W, Ratajeski K, Hankins W B and Glazner A F. 2005. Voluminous granitic magmas from common basaltic sources. *Contributions to Mineralogy and Petrology*, 148(6): 635–661.

Skjerlie K P and Douce A E P. 2002. The fluid-absent partial melting of a zoisite-bearing quartz eclogite from 1.0 to 3.2 GPa; Implications for melting in thickened continental crust and for subduction-zone processes. *Journal of Petrology*, 43(2): 291–314.

Spurlin M S, Yin A, Horton B K, Zhou J and Wang J. 2005. Structural evolution of the Yushu-Nangqian region and its relationship to syncollisional igneous activity, east-central Tibet. *Geological Society of America Bulletin*, 117(9–10): 1293–1317.

Streck M J, Leeman W P and Chesley J. 2007. High-magnesian andesite from Mount Shasta: A product of magma mixing and contamination, not a primitive mantle melt. *Geology*, 35: 351–354.

Sun S S and McDonough W F. 1989. Chemical and isotopic systematics of oceanic basalts: Implications for mantle composition and processes. *Geological Society*, *London*, *Special Publications*, 42(1): 313–345.

Tapponnier P, Zhiqin X, Roger F, Meyer B, Arnaud N, Wittlinger G and Jingsui Y. 2001. Oblique stepwise rise and growth of the Tibet Plateau. *Science*, 294(5547): 1671–1677.

Tchameni R, Mezger K, Nsifa N E and Pouclet A. 2001. Crustal origin of Early Proterozoic syenites in the Congo craton (Ntem complex), South Cameroon. *Lithos*, 57(1): 23–42.

Wang C, Liu Z, Yi H, Liu S and Zhao X. 2002. Tertiary crustal shortening and peneplanation in the Hoh Xil region: Implications for the tectonic history of the northern Tibetan Plateau. *Journal of Asian Earth Sciences*, 20(3): 211–223.

Wang Q, Chung S L, Li X H, Wyman D, Li Z X, Sun W D, Qiu H N, Liu Y S and Zhu Y T. 2012. Crustal melting and flow beneath Northern Tibet: Evidence from Mid-Miocene to Quaternary strongly peraluminous rhyolites in the Southern Kunlun Range. *Journal of Petrology*, 53(12): 2523–2566.

Wang Q, Li J W, Jian P, Zhao Z H, Xiong X L, Bao Z W, Xu J F, Li C F and Ma J L. 2005a. Alkaline syenites in eastern Cathaysia (South China): Link to Permian-Triassic transtension. *Earth and Planetary Science Letters*, 230(3): 339–354.

Wang Q, McDermott F, Xu J F, Bellon H and Zhu Y T. 2005b. Cenozoic K-rich adakitic volcanic rocks in the Hohxil area, northern Tibet: Lower-crustal melting in an intracontinental setting. *Geology*, 33: 465–468.

Wang Q, Wyman D A, Li Z X, Sun W, Chung S L, Vasconcelos P M, Zhang Q Y, Dong H, Yu Y S, Pearson N, Qiu H N, Zhu T X and Feng X. 2010. Eocene north–south trending dikes in central Tibet: New constraints on the timing of east–west extension with implications for early plateau uplift? *Earth and Planetary Science Letters*, 298(1): 205–216.

Wang Q, Wyman D A, Xu J F, Dong Y H, Vasconcelos P M, Pearson N, Wan Y S, Dong H, Li C F and Yu Y S. 2008. Eocene melting of subducting continental crust and early uplifting of central Tibet: Evidence from central-western Qiangtang high-K calc-alkaline andesites,

dacites and rhyolites. *Earth and Planetary Science Letters*, 272: 158–171.

Wang Q, Wyman D A, Xu J F, Zhao Z H, Jian P, Xiong X L, Bao Z W, Li C F and Bai Z H. 2006a. Petrogenesis of Cretaceous adakitic and shoshonitic igneous rocks in the Luzong area, Anhui Province (eastern China): Implications for geodynamics and Cu-Au mineralization. *Lithos*, 89: 424–446.

Wang Q, Xu J F, Jian P, Bao Z W, Zhao Z H, Li C F, Xiong X L and Ma J L. 2006b. Petrogenesis of adakitic porphyries in an extensional tectonic setting, Dexing, South China: Implications for the genesis of porphyry copper mineralization. *Journal of Petrology*, 47: 119–144.

Wu Z H, Barosh P J, Wu Z H, Hu D G, Xun Z and Ye P S. 2008. Vast early Miocene lakes of the central Tibetan Plateau. *Geological Society of America Bulletin*, 120(9–10): 1326–1337.

Xie L W, Zhang Y B, Zhang H H, Sun J F and Wu F Y. 2008. In situ simultaneous determination of trace elements, U-Pb and Lu-Hf isotopes in zircon and baddeleyite. *Chinese Science Bulletin*, 53: 1565–1573.

Xiong X L, Adam J and Green T H. 2005. Rutile stability and rutile/melt HFSE partitioning during partial melting of hydrous basalt: Implications for TTG genesis. *Chemical Geology*, 218(3): 339–359.

Xu J F, Shinjo R, Defant M J, Wang Q and Rapp R P. 2002. Origin of Mesozoic adakitic intrusive rocks in the Ningzhen area of east China: Partial melting of delaminated lower continental crust? *Geology*, 30: 1111–1114.

Yang F Q, Wu H, Pirajno F, Ma B Y, Xia H D, Deng H J, Liu X W, Xu G and Zhao Y. 2007. The Jiashan Syenite in northern Hebei: A record of lithospheric thinning in the Yanshan Intracontinental Orogenic Belt. *Journal of Asian Earth Sciences*, 29(5): 619–636.

Yang J H, Chung S L, Wilde S A, Wu F Y, Chu M F, Lo C H and Fan H R. 2005. Petrogenesis of post-orogenic syenites in the Sulu Orogenic Belt, East China: Geochronological, geochemical and Nd-Sr isotopic evidence. *Chemical Geology*, 214(1): 99–125.

Yang J H, Sun J F, Zhang M, Wu F Y and Wilde S A. 2012. Petrogenesis of silica-saturated and silica-undersaturated syenites in the northern North China Craton related to post-collisional and intraplate extension. *Chemical Geology*, 328: 149–167.

Yin A and Harrison T M. 2000. Geologic evolution of the Himalayan-Tibetan orogen. *Annual Review of Earth and Planetary Sciences*, 28(1): 211–280.

Zhang X M, Teng J W, Sun R M, Romanelli F, Zhang Z J and Panza G F. 2014. Structural model of the lithosphere–asthenosphere system beneath the Qinghai–Tibet Plateau and its adjacent areas. *Tectonophysics*, 634: 208–226.

Zhao W J, Kumar P, Mechie J, Kind R, Meissner R, Wu Z H, Shi D N, Su H P, Xue G Q, Karplus M and Tilmann F. 2011. Tibetan plate overriding the Asian plate in central and northern Tibet. *Nature Geoscience*, 4(12): 870–873.

Geochronology, Geochemistry and Petrogenesis of the Eocene Qoimaco Quartz-monzonites in Qiangtang Area

ZENG Jipeng[1, 2], WANG Qiang[1*], OU Quan[1], QI Yue[1], HAO Lulu[1], SUN Peng[1], WANG Jun[1] and CHEN Yiwei[1]

(1. *State Key Laboratory of Isotope Geochemistry*, *Guangzhou Institute of Geochemistry*, *Chinese Academy of Sciences*, *Guangzhou* 510640, *Guangdong*, *China*; 2. *University of Chinese Academy of Sciences*, *Beijing* 100049, *China*)

Abstract: Syenite and alkali-rich quartz-monzonite are generally considered to be derived from partial melting of the enriched mantle. This paper reports quartz-monzonites derived from partial melting of thickened continental crust. The Qoimaco pluton is located at the Qoima Mountain, Northeast of the Qoimaco Lake in the northern Qiangtang (central Tibetan Plateau). The pluton was regarded as mainly consisting of syenite porphyries with formation age of 45 to 23 Ma. Our recent detailed field geological investigation, petrological, geochemical and geochronological studies demonstrated that the pluton mainly consists of quartz-monzonite, and has zircon U-Pb age of 41.71±0.29 Ma, simultaneously with the Eocene volcanic lavas in the area. The rocks have high SiO_2 (65.12%–66.71%), Al_2O_3 (>14.79%), and alkali (Na_2O+K_2O, 9.08%–9.71%), K_2O (5.50%–5.92%), Sr (1874–2001 μg/g), and Sr/Y (124–136) and La/Yb (67–74) ratios. The rocks are characterized by depleted heavy rare earth elements (e.g., Yb=1.24–1.34 μg/g), Y (14.4–15.7 μg/g) and high field strength elements, enriched large ion lithophile elements, and negligible Eu and Sr anomalies and slightly high $Mg^{\#}$ values (47–56). The major and trace element features of the rocks are similar to those of the contemporary adakitic volcanic lavas in the area. In addition, the rocks have very uniform initial $^{87}Sr/^{86}Sr$ ratios (~0.7069) and $\varepsilon_{Nd}(t)$ values (from −2.6 to −2.8). Considering the regional geological, petrological and tectonic data, we suggest that the Qoimaco quartz-monzonites were generated through partial melting of the subducted crust during intra-continent subduction, which subsequently interacted with the mantle peridotite during ascent, in the compression setting in the central Tibet triggered by India-Asia continental collision.

Keywords: quartz-monzonites; adakitic rocks; thickened lower crust; Eocene; Qiangtang; Tibet Plateau